Journal of Theoretical and Applied Mechanics, Sofia, 2008, vol. 38, Nos 1–2, pp. 45–60

LARGE DEFORMATION ANALYSIS USING A QUASI-STATIC MATERIAL POINT METHOD

L. Beuth, T. Benz, P. A. Vermeer
Universität Stuttgart,
Pfaffenwaldring 35, 70569 Stuttgart, Germany,
e-mail: lars.beuth@igs.uni-stuttgart.de

Z. Więckowski
Technical University of Łódź,
6, al. Politechniki, 90-924 Łódź, Poland

[Received 16 October 2007. Accepted 25 February 2008]

Abstract. The Finite Element Method (FEM) has become the standard tool for the analysis of a wide range of solid mechanics problems. However, the underlying structure of a classical updated Lagrangian FEM is not well suited for the treatment of large deformation problems, since excessive mesh distortions can lead to numerical difficulties. The Material Point Method (MPM) represents an approach in which material points moving through a fixed finite element grid are used to simulate large deformations. As the method makes use of moving material points, it can also be classified as a point-based or meshless method. With no mesh distortions, it is an ideal tool for the analysis of large deformation problems. MPM has its origin in fluid mechanics and has only recently been applied to solid mechanics problems. It has been used successfully for impact analyses where bodies penetrate each other and for silo discharging problems. All existing MPM codes found in literature are dynamic codes with explicit time integration and only recently implicit time integration. In this study a quasi-static MPM formulation and implementation are presented. The paper starts with the description of the quasi-static governing equations and the numerical discretisation. Afterwards, the calculation process of the quasi-static MPM is explained, followed by the presentation of some geotechnical boundary value problems which have been solved with the newly developed quasi-static MPM code. The benchmark problems consist of an oedometer test and a slope. For validation, the results are compared with analytical solutions and FEM results, respectively.
Key words: meshless methods, Material Point Method, large deformations.

1. Introduction

Over the last 25 years, the Finite Element Method (FEM) has become a standard tool for the analysis of a wide range of solid mechanics problems. However, FEM is not well suited for the modelling of large deformation problems. When these problems are modelled with an updated Lagrangian Finite Element Method, considerable mesh distortions occur, which require remeshing. During the remeshing process all the state variables have to be mapped from the distorted mesh to the newly defined mesh, which introduces errors [1].

To overcome the difficulties of FEM, so-called meshless methods have been developed, for example, the Element-Free Galerkin Method and Smoothed Particle Hydrodynamics [2]. The Material Point Method (MPM) might be classified as a meshless method, a particle method or an Arbitrary Lagrangian-Eulerian (ALE) method [3].

MPM uses two discretizations of the material, one based on a computational mesh and the other based on a collection of material points or "particles". All the properties of the continuum (material data and deformation state) as well as the external loads are carried by the material points, while the grid carries no permanent information. The computational grid is used to determine incremental displacements by solving the governing equations as with the standard finite element method. With the MPM large deformations are modelled by moving material points through the mesh. By this approach, MPM combines the advantages of both Eulerian and Lagrangian formulations.

The early beginnings of MPM can be traced back to the work of Harlow [4], who studied fluid flow by material points moving through a fixed grid. Sulsky *et al.* [5] later extended the approach to the modelling of solid mechanics and called it the Material Point Method. Bardenhagen *et al.* [6] extended the method further to include frictional contact between deformable solid bodies.

The potential of MPM of simulating granular flow was first recognised by Więckowski [7]. Several papers on MPM modelling of silo discharge were published [3, 7, 8]. Coetzee [9] and Coetzee *et al.* [10] extended the method to include a micro-polar Cosserat continuum for studying anchor pull-out and the large deformation problem of excavator bucket filling.

Most MPM implementations developed so far are dynamic codes which employ an explicit time integration scheme. Although it is possible to use these programs also for the analysis of quasi-static problems, this is computationally inefficient as explicit integration requires very small time steps and can lead to long computation times. For these reasons, it was decided to develop a

quasi-static MPM implementation which uses an implicit integration scheme, thereby broadening the possibilities of large deformation analyses for complex, large-scale geotechnical problems.

MPM is based on FEM so that many of the standard FEM routines can be used. The MPM code presented in this paper is based on an existing updated Lagrangian FEM code [11].

2. Quasi-static MPM formulation

In this section the field equations of quasi-static large deformation are presented. It is followed by a description of the numerical scheme.

2.1. Field equations of quasi-static deformation

The internal static equilibrium of a continuum can be written as

$$\frac{\partial \sigma_{ij}}{\partial x_j} + \gamma_i = 0, \tag{1}$$

and on the external boundary S as

$$\tau_i = \sigma_{ij} \cdot n_j, \qquad i, j, k = 1, 2, 3, \tag{2}$$

where x_j are Cartesian coordinates, σ_{ij} denotes the Cauchy stress tensor, γ_i represents body forces and τ_i denotes the boundary traction components.

Applying Galerkin's variational principle followed by integration by parts (Green's theorem) yields the equilibrium equation in the weak form

$$\int_V \sigma_{ij} \cdot \frac{\partial \delta u_i}{\partial x_j} dV = \int_V \gamma_i \cdot \delta u_i dV + \int_S \tau_i \cdot \delta u_i dS, \tag{3}$$

where δu_i represents a kinematically admissible variation of displacements, i.e. a virtual displacement.

The development of the stress state σ_{ij} can be regarded as an incremental process

$$\sigma_{ij} = \sigma_{ij}^0 + \Delta\sigma_{ij}. \tag{4}$$

In this relation σ_{ij} represents the actual state of stress at the end of a load step and σ_{ij}^0 represents the previous state of stress at the beginning of this particular load step. Equation (3) can now be written as

$$\int_V \Delta\sigma_{ij} \cdot \frac{\partial \delta u_i}{\partial x_j} dV = \int_V \gamma_i \cdot \delta u_i dV + \int_S \tau_i \cdot \delta u_i dS - \int_V \sigma^0_{ij} \cdot \frac{\partial \delta u_i}{\partial x_j} dV. \tag{5}$$

So far, the final configuration for x_i and V is taken as a reference configuration. However, at the beginning of an increment, this configuration is not known. Therefore, equation (5) is reformulated so that the variables of the initial geometry x^0_i and V^0 of a load step are used as the reference configuration

$$\begin{aligned} &\int_{V_0} \Delta\Sigma_{ji} \cdot \frac{\partial \delta u_i}{\partial x^0_j} dV_0 \\ &= \int_{V_0} \gamma_i \cdot \delta u_i dV_0 + \int_{S_0} \tau_i \cdot \delta u_i dS_0 - \int_{V_0} \sigma^0_{ij} \cdot \frac{\partial \delta u_i}{\partial x^0_j} dV_0 + \text{Higher Order Terms}, \end{aligned} \tag{6}$$

where Σ_{ji} is the first Piola-Kirchoff stress tensor. The increment of the first Piola-Kirchoff stress tensor can be written as

$$\Delta\Sigma_{ji} = \Delta\sigma_{ji} - \sigma^0_{ki} \cdot \frac{\partial \Delta u_j}{\partial x^0_k} + \sigma^0_{ji} \cdot \frac{\partial \Delta u_k}{\partial x^0_k}. \tag{7}$$

Due to the second term, this stress rate is non-symmetric. The Cauchy stress increment $\Delta\sigma_{ij}$ can be written as

$$\Delta\sigma_{ij} = \Delta\sigma^J_{ij} + \sigma^0_{ik} \cdot \Delta\omega_{kj} + \sigma^0_{jk} \cdot \Delta\omega_{ki}, \tag{8}$$

where $\Delta\sigma^J_{ij}$ is the Jaumann stress rate. The incremental strains $\Delta\varepsilon_{ij}$ and rotations $\Delta\omega_{ij}$ are given by

$$\Delta\varepsilon_{ij} = \frac{1}{2}\left(\frac{\partial \Delta u_i}{\partial x^0_j} + \frac{\partial \Delta u_j}{\partial x^0_i}\right), \tag{9}$$

$$\Delta\omega_{ij} = \frac{1}{2}\left(\frac{\partial \Delta u_j}{\partial x^0_i} - \frac{\partial \Delta u_i}{\partial x^0_j}\right). \tag{10}$$

The constitutive relation between the Jaumann stress increment and the strain increment is

$$\Delta\sigma_{ij}^{J} = \overset{\cdot}{D}_{ijkl}\Delta\varepsilon_{kl} - \sigma_{ij}^{0} \cdot \Delta\varepsilon_{kk}, \tag{11}$$

where D_{ijkl} is the elastic element stiffness matrix. The left hand side of equation (6) now becomes

$$\int_{V_0} D_{ijkl}^{0} \cdot \Delta\varepsilon_{kl} \cdot \delta\varepsilon_{ij} dV_0 + \int_{V_0} \left[\sigma_{ki}^{0} \cdot \Delta u_{j,k} \cdot \delta u_{j,i} - 2 \cdot \sigma_{ki}^{0} \cdot \Delta\varepsilon_{jk} \cdot \delta\varepsilon_{ij}\right] dV_0 = \text{Right Hand Side}, \tag{12}$$

where the first term is the usual (small strain) internal virtual work and the second term contains the large deformation contribution [12].

2.2. Numerical scheme

The element mesh used within the MPM is identical to a FEM mesh. Interpolation functions are used to interpolate nodal values to the interior of an isoparametric element. Making use of matrix notation, the displacement field $\Delta\underline{u}$, for example, is given by

$$\Delta\underline{u} = \underline{\underline{N}}\,(\xi, \eta, \zeta) \cdot \Delta\underline{v}, \tag{13}$$

where $\Delta\underline{v}$ is the nodal displacement vector, $\underline{\underline{N}}$ is assembled from shape functions and ξ, η and ζ are the local coordinates, respectively.

The strains at any point within the finite elements are determined from the nodal displacements $\Delta\underline{v}$

$$\Delta\underline{\varepsilon} = \underline{\underline{L}} \cdot \Delta\underline{u} = \underline{\underline{L}} \cdot \underline{\underline{N}} \cdot \Delta\underline{v} = \underline{\underline{B}} \cdot \Delta\underline{v}, \tag{14}$$

where $\underline{\underline{L}}$ contains the Cartesian differential operators and $\underline{\underline{B}}$ denotes the well-known strain interpolation matrix.

Making use of these definitions, the equilibrium equation, given by equation (12), now becomes

$$\left[\underline{\underline{K}}^{E} + \underline{\underline{K}}^{G}\right] \cdot \Delta\underline{v} = \underline{f}_{\text{ load}} - \underline{f}_{\text{ internal}} + \text{Higher Order Terms}, \tag{15}$$

where the elastic stiffness matrix is given by

$$\underline{\underline{K}}^E = \int_{V_0} \underline{\underline{B}}^T \cdot \underline{\underline{D}} \cdot \underline{\underline{B}} dV_0, \tag{16}$$

and the geometric stiffness matrix is determined from the stresses $\underline{\sigma}^0$ at the beginning of the load step

$$\underline{\underline{K}}^G_{qp} = \int_{V_0} \left[L_{jpk} \cdot \sigma^0_{ki} \cdot L_{jqi} - 2 \cdot B_{jpk} \cdot \sigma^0_{ki} \cdot B_{iqj} \right] dV_0 \tag{17}$$

with $L_{ijk} = N_{ij,k}$ and

$$B_{ijk} = \frac{1}{2} \cdot \left[L_{ijk} + L_{kji} \right]. \tag{18}$$

The external load vector contains body forces and surface tractions

$$\underline{f}_{\text{ load}} = \underline{f}_{\text{ body}} + \underline{f}_{\text{ traction}} = \int_{V_0} \underline{\underline{N}}^T \cdot \underline{\gamma} dV_0 + \int_{S_0} \underline{\underline{N}}^T \cdot \underline{\tau} dS_0, \tag{19}$$

while the internal (reaction) force vector is given by

$$\underline{f}_{\text{ internal}} = \int_{V_0} \underline{\underline{B}}^T \cdot \underline{\sigma} dV_0. \tag{20}$$

Because of the higher-order terms on the right hand side, equation (15) has to be solved iteratively as described in the following section.

In standard FEM, Gauss-Legendre integration is used to integrate the stiffness terms over the element volume with a fixed number of integration points. In MPM, the integration is performed over the (changing) volume Ω_p of the element material points.

3. MPM calculation process

In MPM, a set of material points is tracked throughout the deformation history of a body. The full numerical solution is calculated at these material

points. Global position, stress and strain, for example, are associated with these material points.

The calculation process of the quasi-static MPM can be divided into three steps:

During the *Initialisation Phase*, the initial values of quantities assigned to material points are set from initial data defining the given problem. The information carried by the material points is projected onto a background finite element mesh where equations of equilibrium are solved in an updated Lagrangian frame. Information from this solution is then used to update the material points.

The solution on the mesh is called the *Lagrangian Phase* of the calculation. Once the material points have been updated, the mesh is reset to its initial configuration. The movement of the mesh relative to the material points models convection, and is called the *Convective Phase* of the calculation [5].

With reference to the equations given in the previous section, each of the MPM calculation phases is described in more detail.

3.1. The Initialisation Phase

This phase starts by generating a finite element mesh. In contrast to FEM, the mesh is not only generated where material exists, but over the complete domain where material is expected to move.

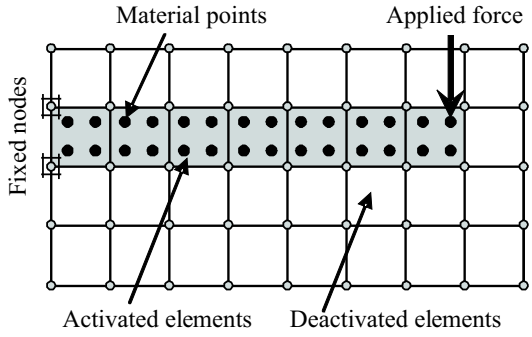

Fig. 1. Initialisation Phase

Material points are placed inside elements to form (define) the solid body. This is shown in Fig. 1, for the simple case of a cantilever. Elements containing material points are called *activated elements* and elements containing no material points are called *deactivated elements*. As material points move

through the grid, elements become activated and deactivated using a special house-keeping algorithm. Similar to FEM, constraints are handled by fixing nodes, i.e. zero displacements are enforced at these nodes (Fig. 1).

During the Initialisation Phase, loads are assigned to material points which they carry throughout the deformation process. The material points are initially evenly distributed in an element, and thus each gives the same volume.

In the 3D code presented in this paper, 6-noded wedge elements were used with linear shape functions [11] and initially 8 material points per element, each with a weight of $\omega_p = 1/8$.

3.2. The Lagrangian Phase

With all the state variables initialised at material points during the Initialisation Phase, the Lagrangian Phase can be executed. The result of the Lagrangian Phase are nodal displacement increments solved through an iterative procedure. The formulation of the iterative procedure starts with the linearized equilibrium equation (equation (15))

$$\left[\underline{\underline{K}}^E + \underline{\underline{K}}^G\right]^0 \cdot \Delta\underline{v} = \underline{f}_{\text{load}} - \underline{f}^0_{\text{internal}}. \tag{21}$$

The iterative procedure reads

$$\left[\underline{\underline{K}}^E + \underline{\underline{K}}^G\right]^0 \cdot \delta\underline{v}^k = \underline{f}_{\text{load}} - \underline{f}^{k-1}_{\text{internal}}, \tag{22}$$

where $k = 1, 2, \ldots, n$ is the iteration number of the load step considered. Sub-displacement increments (sub-increments) $\delta\underline{v}$ are solved and added together to form the nodal displacement increments

$$\Delta\underline{v}^k = \sum_{l=1}^{k} \delta\underline{v}^l. \tag{23}$$

The initial value of $\underline{f}^{k-1}_{\text{internal}}$ for $k = 1$ is given by

$$\underline{f}^0_{\text{internal}} = \int_V \underline{\underline{B}}^T \underline{\sigma}^0 dV \tag{24}$$

with subsequent values of $\underline{f}_{\text{internal}}$ computed from

$$\underline{f}^{k}_{\text{internal}} = \int_{V} \underline{\underline{B}}^{T} \underline{\sigma}^{k} dV, \tag{25}$$

where the stress update is given by

$$\Delta\sigma_{ij} = D_{ijkl} \cdot \Delta\varepsilon_{kl} - \sigma_{ij} \cdot \Delta\varepsilon_{kk} + \sigma^{0}_{ik} \cdot \Delta\omega_{kj} + \sigma^{0}_{jk} \cdot \Delta\omega_{ki}. \tag{26}$$

The number of iterations is stopped as soon as

$$\left\| \underline{f}_{\text{load}} - \underline{f}^{k}_{\text{internal}} \right\| \leq \alpha \cdot \left\| \underline{f}_{\text{load}} \right\|, \tag{27}$$

where α is a specified tolerance, e.g. $\alpha = 0.01$.

3.3. The Convective Phase

At the end of the Lagrangian Phase, the nodal displacements $\Delta\underline{v}$ are known as shown in Fig. 2(b). The mesh is now reset to its initial configuration as shown in Fig. 2(c), while the material points keep their global positions. The house-keeping algorithm now determines which elements should be activated and which should be deactivated.

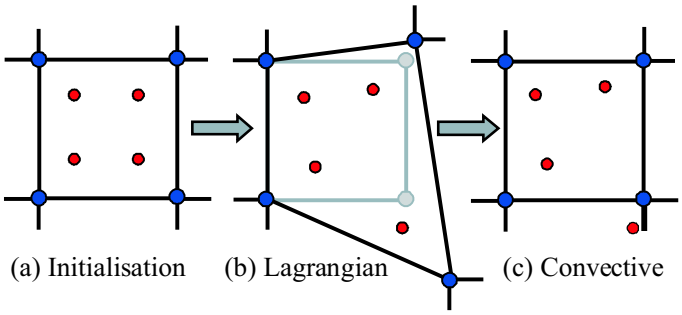

Fig. 2. The MPM calculation process: Initialisation Phase, Lagrangian Phase and Convective Phase

The material point volumes Ω_p are updated using

$$\Omega^{i}_{p} = \omega^{i-1}_{p} \cdot \frac{\left|J^{i-1}_{p}\right|}{\left|J^{0}_{p}\right|} \cdot \left|J^{i}_{p}\right|, \tag{28}$$

where J_p is the Jacobian matrix evaluated at the material point position.

The mass of each material point, used for calculating the body forces, is calculated by

$$m_p = \rho \cdot \Omega_p, \tag{29}$$

where ρ is the material density assigned to the material point.

4. Benchmark problems

4.1. Oedometer test

The oedometer test is a standard geotechnical laboratory test. It provides a one-dimensional deformation problem which can easily be checked for accuracy using an analytical solution. The analytical solution for the one-dimensional compression of an elastic material is based on the logarithmic strain measure for large deformations [12]

$$\varepsilon_L = -\ln\left(\frac{L}{L_0}\right), \tag{30}$$

where ε_L is the logarithmic strain, L_0 the initial height and L is the deformed height of the soil sample in the oedometer. With

$$\frac{L}{L_0} = 1 - \frac{\Delta L}{L_0} = 1 - \varepsilon, \tag{31}$$

the formula for the logarithmic strain ε_L can also be written as

$$\varepsilon_L = -\ln\left(1 - \varepsilon\right), \tag{32}$$

where ε is the (vertical) engineering strain. For small deformations up to $\varepsilon \approx 0.1$ the logarithmic strain is virtually equal to the engineering strain. Strains above this limit are considered as large deformations.

Van Langen [12] derived the analytical solution for the Cauchy stress σ as follows: $\sigma = E \cdot [e^{\varepsilon_L} - 1]$. For small values of ε_L this equation simply reduces to $\sigma = E \cdot \varepsilon_L$. The deviation from this linear equation is caused by the fact that Van Langen assumes a linear relation between the Kirchoff stress Σ^K and the logarithmic strain ε_L, i.e. $\Sigma^K = E \cdot \varepsilon_L$, where E is the Young's modulus.

In Figure 3 the stress-strain curve obtained from a MPM calculation of the oedometer problem is plotted versus Van Langen's analytical solution. In the MPM calculation a mesh with a total of 16 6-noded wedge elements with linear interpolation functions is used (Fig. 3). All elements are initialised with 8 material points each so that all particles represent the same material volume. Figure 3 shows a stress-strain curve plotted in for a material point near the centre of the specimen, which shows that MPM results agree quite well with the analytical solution.

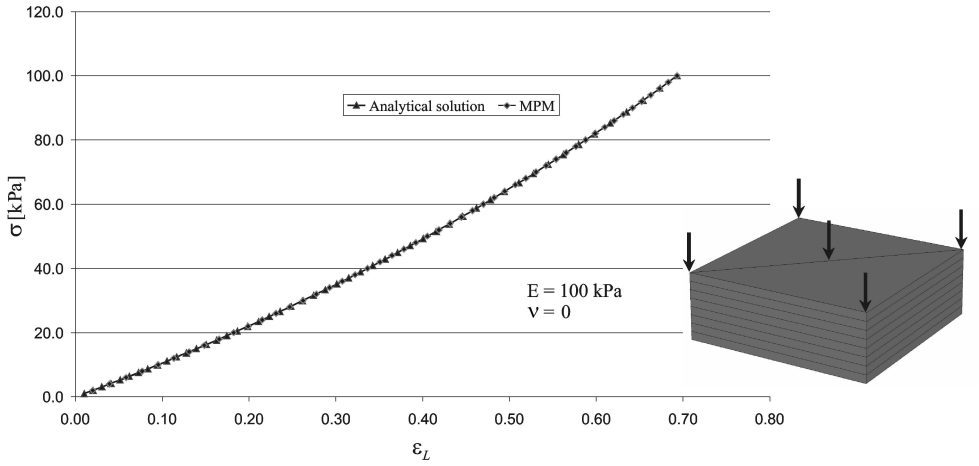

Fig. 3. Computed oedometer stress-strain curve (MPM) versus van Langen's analytical solution

4.2. Slope problem

The second benchmark problem consists of a slope with an inclination of 45° and a height of 1 m; Figure 4 presents the geometry of the problem. The same boundary value problem was analysed by Ernst [13] using a linear elastic perfectly plastic model with Mohr-Coulomb failure envelope with a cohesion of $c = 1$ kPa, a friction angle of $\phi = 25°$, a dilatancy angle $\psi = 0°$, and a Poisson's ratio of $\nu = 0.33$. Ernst studied the slope response under gravity loading and as computational result he plotted the unit weight of the soil γ as a function of vertical displacement for the point located at the top of the slope, marked as "A" in Fig. 4. As the currently developed MPM code is a full 3D code, the plane strain problem is analysed in a 3D slice as shown in Fig. 5. The mesh provided within the MPM Initialisation Phase (see Section 3.1) is shown on the right hand side of Fig. 5.

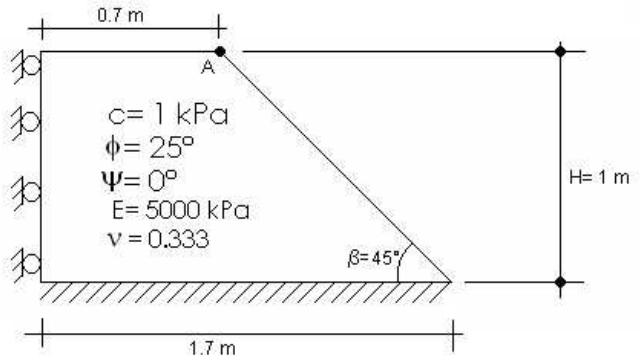

Fig. 4. Slope problem: geometry and material parameters after [13]

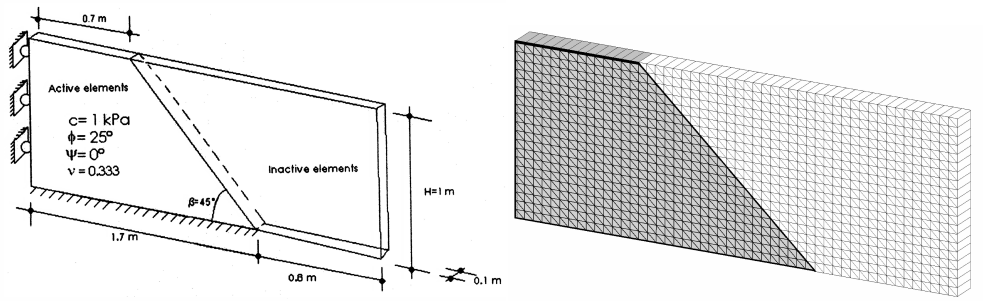

Fig. 5. Slope problem: 3D geometry (left) and initial configuration highlighting the activated elements (right) in the MPM analysis

The load-displacement curves calculated with MPM are compared with the results from updated Lagrangian FEM simulations. In Figure 6, the vertical displacement u of the crest point A is multiplied by the Young's modulus used in the respective calculation. Calculations are carried out for Young's moduli of 50 kPa and 200 kPa. The resulting displacements are proportional to 1/E, meaning that any value of Young's modulus may be chosen, provided that this value is used to normalize resulting displacements, as shown in Fig. 6. For the FEM calculations, the same 15-noded wedge elements with quadratic interpolation functions are used as in the MPM analysis. The Mohr-Coulomb criterion serves as failure criterion for the linear elastic – perfectly plastic constitutive material law used.

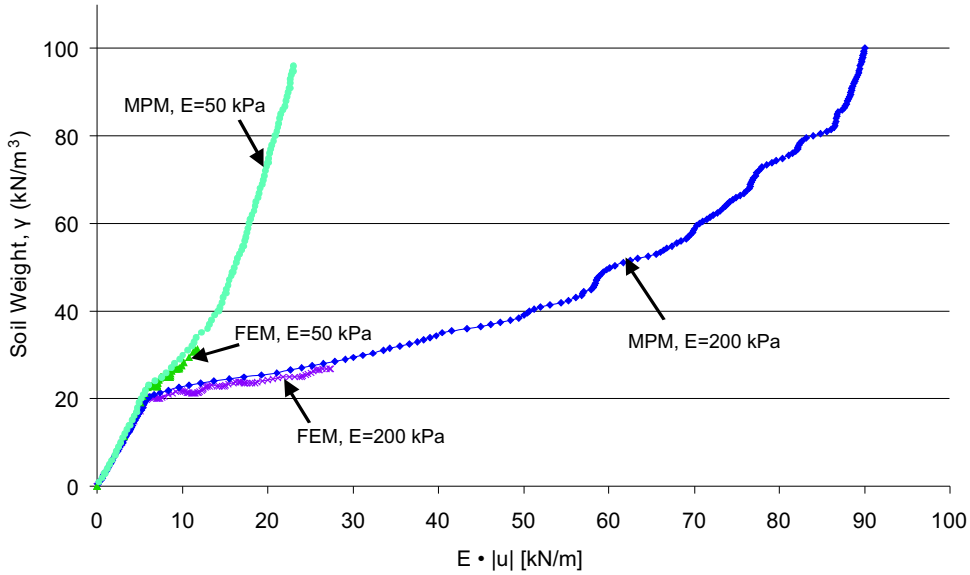

Fig. 6. Load-displacement curves (Point A) for $E = 50$ kPa and $E = 200$ kPa

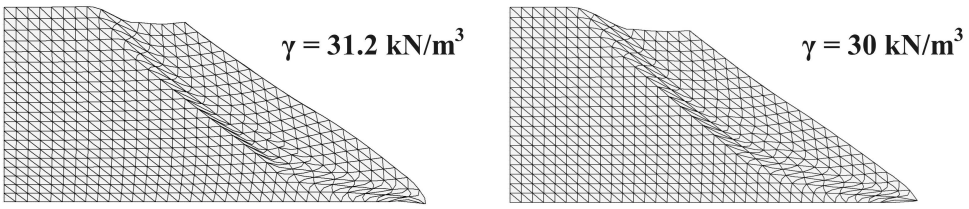

Fig. 7. FEM Slopes at failure: $E = 50$ kPa (left) and $E = 200$ kPa (right)

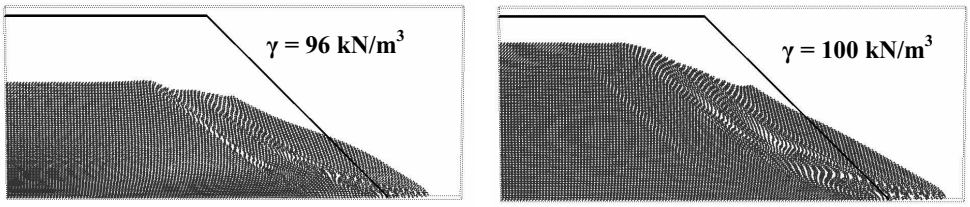

Fig. 8. MPM Slopes, final configurations: $E = 50$ kPa (left) and $E = 200$ kPa (right)

Both FEM and MPM analyses yield practically the same load displacement curves as long as the material behaves mostly elastic. For plastic material behaviour, the MPM and FEM load-displacement curves are slightly different, with the MPM predicting a somewhat stiffer response than the FEM. The MPM response can be attributed to material that makes contact with the lower boundary beyond the slope toe. This additional support cannot be modelled with the FEM in the same manner. The most striking difference between the FEM and MPM curves is the capacity of MPM to produce physical results up to very large deformations. FEM meshes become highly distorted when material weights exceed $\gamma = 30$ kN/m^3, and FEM results are no longer reliable. By contrast, MPM calculations can be continued all the way until particles reach the boundaries of the defined mesh, with material weight reaching $\gamma = 100$ kN/m^3 or so.

To test sensitivity to mesh refinement, MPM calculations were run on meshes of varying coarseness, shown in Fig. 9. The load-displacement curves of the control point A, shown in Fig. 10, demonstrate that mesh refinement has a significant impact on the calculation of this slope. Therefore, it is planned to implement a regularization method in the future.

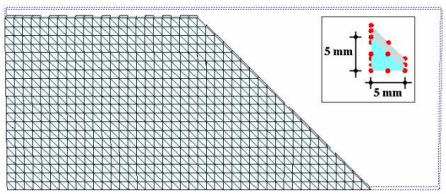

(a) Fine mesh, with 9808 nodes

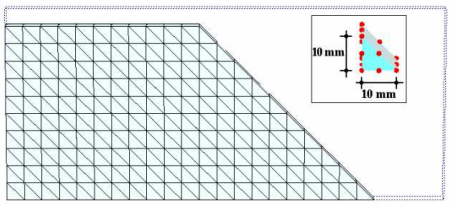

(b) Medium mesh, with 2658 nodes

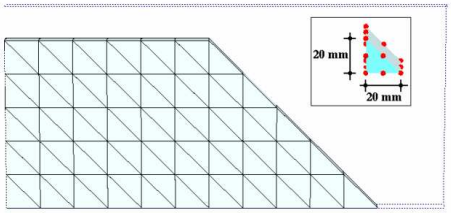

(c) Coarse mesh, with 800 nodes

Fig. 9. Meshes of increasing coarseness

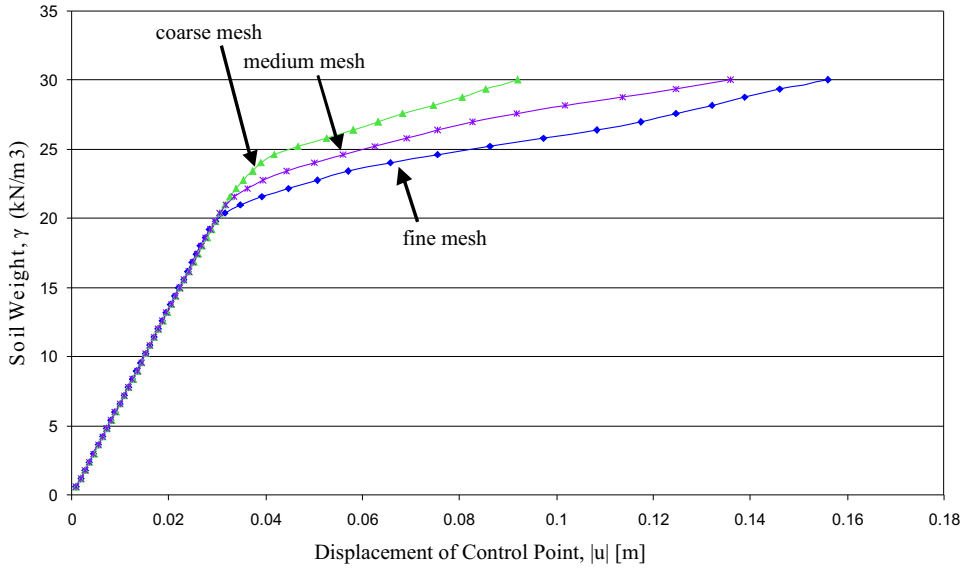

Fig. 10. High-order MPM sensitivity to mesh refinement

5. Conclusions

The development of a three-dimensional quasi-static MPM code is presented. MPM can model large deformations without the risk of numerical instability caused by extensive mesh distortions, and without the high computational costs of remeshing. The code was implemented using an existing updated Lagrangian FEM code. Results from an oedometer test and a slope problem are compared to an analytical model and FEM results, respectively.

It is shown that MPM can model the large deformations of an oedometer. The calculated stress-strain curve is in agreement with the analytical solution. It is also shown that MPM can model the failure of a slope. The calculated load-displacement curves correspond well with the results from FEM for the almost elastic branch of the loading process. Thereafter, MPM predicts displacements slightly less than those obtained from FEM. This is considered a physical result as the displaced material points may give additional support at the slope toe. FEM capacity to model material deformation is limited by distortions in the FEM mesh, while MPM calculations can be continued and produce reliable results up to very large deformations.

In the current MPM, 15-noded wedge elements with second-order interpolation functions are used, as this yields more accurate results than with

6-noded elements. In this paper, the material was assumed to be linear elastic–perfectly plastic; in the future, hardening plasticity will be added.

It is concluded that MPM is well suited for the modelling of large deformation problems. Geotechnical applications such as pile driving, installation of spudcans, and bucket foundations will be investigated in the near future.

REFERENCES

[1] Więckowski, Z. The Material Point Method in Large Strain Engineering Problems. *Computer Methods in Applied Mechanics and Engineering*, **193** (2004), 4417–4438.

[2] Li, S., W. K. Liu. Meshfree and Particle Methods and Their Applications. *Appl. Mech. Re*, **55** (2002), No. **1**.

[3] Więckowski, Z., S. K. Youn, Y. H. Yeon. A Particle-in-Cell Solution to the Silo Discharging Problem. *Int. J. Numer. Meth. Engng*, **45** (1999), 1203–1225.

[4] Harlow, F. H. The Particle-in-Cell Computing Method in Fluid Dynamics. *Methods in Computational Physic*, **3** (1964), 319–343.

[5] Sulsky, D., H. L. Schreyer. Axisymmetric Form of the Material Point Method with Applications to Upsetting and Taylor Impact Problems. *Comput. Methods Appl. Mech. Engrg*, **139** (1996), 409–429.

[6] Bardenhagen, S. G., J. U. Brackbill, D. Sulsky. The Material-Point Method for Granular Materials. *Computational Methods in Applied Mechanics and Engineering,* **187** (2000), 529–541.

[7] Więckowski, Z. A Particle-in-Cell Method in Analysis of Motion of a Granular Material in a Silo, Computational Mechanics: New Trends and Applications, CIMNE, Barcelona, 1998.

[8] Więckowski, Z. Modelling of Silo Discharge and Filling Problems by the Material Point Method. *Task Quarterly*, **4** (2003), 701–721.

[9] Coetzee, C. J. The Modelling of Granular Flow Using the Particle-in-Cell Method, PhD Thesis, Department of Mechanical Engineering, University of Stellenbosch, South Africa, 2004.

[10] Coetzee, C. J., P. A. Vermeer, A. H. Basson. The Modelling of Anchors Using the Material Point Method. *International Journal for Numerical and Analytical Methods in Geomechanics*, **29** (2005), 879–895.

[11] Plaxis, B. V. Plaxis 3D Foundation Scientific Manual, Version 1.5, 2006.

[12] Van Langen, H. Numerical Analysis of Soil-Structure Interaction, PhD Thesis, Faculty of Civil Engineering, Delft University of Technology, 1991.

[13] Ernst, R. De stabiliteit van eenvoudige taluds, glijvlakberekening versus elementen-method, PhD Thesis, Technical University of Delft, 1983.